Proceedings of the Estonian Academy of Sciences,
2014, **63**, 3, 346–354
doi: 10.3176/proc.2014.3.09
Available online at www.eap.ee/proceedings

BIOMEDICAL
ENGINEERING

# Weak electron emission current for characterization of nanomaterials, gas and radiation sensing towards medical applications

Yuri Dekhtyar

Riga Technical University, Kalku 1, LV1658, Riga, Latvia; jurijs.dehtjars@rtu.lv

Received 25 February 2014, accepted 22 April 2014, available online 28 August 2014

**Abstract.** Rapid development of nanomaterials opens a wide horizon for their applications, medicine being one of them. Nanomaterials and nanodevices are in use both in the human body and as medical nanosensors. Reliable employment of materials requires trustworthy detection of their properties. Characterization of both the nanomaterials and nanosensors should be supplied at the nanoscaled dimension. To avoid disturbing gentle nanoobjects, measurements of them with contactless techniques are preferable. Low energy electron has a mean free path in a solid that is of the order of nanoscale. Therefore, a prethreshold (energy of the emitting electron is close to the electron work function) electron emission contactless spectroscopy could become an efficient instrument both for characterization of nanostructured materials and nanosensing. Weak emission ($\sim 10^{-16} \ldots 10^{-15}$ Q/cm$^2$) of electrons from a solid does not give a significant feedback to measurements in the sense of the negligible inducted electrical charge at the material surface (the density of the surface electrons in the solid is around $10^{14}$ cm$^{-2}$). The paper reviews photo-, dual-, and exo-electron emission fundamentals and their applications for the characterization of nanoobjects (concentration of pointlike imperfections, their annealing, migration, surface charge of nanoparticles, energy gap, electron density of states, thickness of thin films and interfaces between them and the substrate) as well as gas and ionizing radiation. The ways for medical applications are indicated.

**Key words:** nanoobjects, nanosensing, gas, radiation, prethreshold weak electron emission.

## 1. INTRODUCTION

Rapid development of nanotechnologies opens a wide horizon for applications of nanomaterials and nanodevices in different fields, medicine being one of them. Nanomaterials and nanodevices are in use both in the human body, as medical sensors, etc. Advances of local radiation therapy technologies provide the necessity of nanodosimetry (dose measurement at the nanovolume), that could be achieved, when the dosimeter is fabricated from the nanostructured material. Medical applications of nanomaterials, including their characterization, and provision of nanosensors are under fast development. Alongside with that, nanodosimetry is going ahead, too. The above trends are characterized by a rising number of publications in the corresponding area (Fig. 1).

Reliable employment of materials requires trustworthy detection of their properties. To avoid disturbing gentle nanoobjects the contactless characterization is preferable. The present review focuses on a low energy electron weak emission to demonstrate its possibilities for the contactless technique to characterize nanoobjects, chemical and radiation sensing for medical applications.

Low energy (a couple of eV or less) electron has a mean free path in a solid that is in order of nanoscale. To

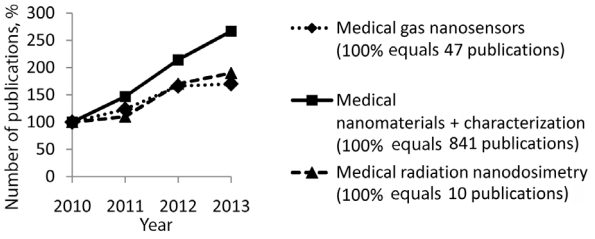


**Fig. 1.** Annual number of publications (Scopus data base) related to the key words: *medical gas sensors*, *medical radiation nanodosimetry*, *medical nanomaterials*, and *characterization* [1–3].

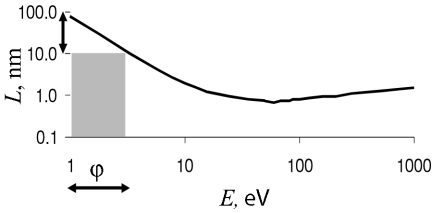


**Fig. 2.** The magnitude of the electron mean free path in a solid material as a function of $E$ [5].

provide emission of such electrons they should be excited at the prethreshold mode, when the energy of the emitting electron is slightly higher than the electron work function (an energy threshold to escape the electron). In this case, the energy $(E)$ of the energized electron is just several eV [4] and its mean free path $(L)$ in the solid corresponds to the nanodimension (Fig. 2) [5].

## 2. FUNDAMENTALS OF THE PRETHRESHOLD ELECTRON EMISSION

### 2.1. Photoelectron emission

The current $(I)$ of the prethreshold single photon excited electron emission (photoelectron emission) is described by the classical formula

$$I = K(h\nu - \varphi)^m, \tag{1}$$

where $K$ is a coefficient, $h\nu$ is the energy of the exciting photon, and $\varphi$ is the electron work function.

For the prethreshold emission mode $(h\nu \geq \varphi)$, the values of $\varphi$ are equal to several units of eV (~5 eV) [4], and therefore $L$ of the photoelectron within the emitter is around 10–100 nm (Fig. 2). To emit the electron, it is excited from the initial (i) to the final (f) energy state that correspond to the energies $E_{\mathrm{i}}$ and The emission current is given as [6]:

$$I \sim \int_0^W N_{\mathrm{i}}(E) N_{\mathrm{f}}(E, h\nu)\,\mathrm{d}E, \tag{2}$$

where $N_{\mathrm{i}}, N_{\mathrm{f}}$ denote the density of the initial and final electron states, correspondingly.

The energy of the emitted electron above the vacuum energy level, $W$, can be expressed as

$$W = E_{\mathrm{f}} - E_{\mathrm{vac}} = h\nu + E_{\mathrm{i}} - E_{\mathrm{vac}},$$

where $E_{\mathrm{vac}}$ is the energy of the vacuum level.

When emission of electrons is provided from the local state $(E_i = \mathrm{const})$, one could find [7] that

$$\frac{\mathrm{d}I}{\mathrm{d}W} \sim N_{\mathrm{i}}(W) N_{\mathrm{f}}(W, h\nu),$$

or

$$\frac{\mathrm{d}I}{\mathrm{d}(h\nu)} \sim N_{\mathrm{i}}(W) N_{\mathrm{f}}(W, h\nu). \tag{3}$$

The formula (3) gives an instrument to estimate electron density of states, if the emission current is measured as a function of $h\nu$.

The electron work function in the case of emission from metals and semimetals that do not have an energy gap $(E_g)$ is equal to the electron affinity $\chi$. For the materials with $E_g$ (semiconductors, dielectrics):

$$\varphi = E_g + \chi.$$

As noted in [8], $m > 1$ in the majority of electron transitions caused by the photons. This means that a small increment of $\varphi$, stipulated by a surface charge, and reconstruction of the electron density of states, etc., influence $I$ very strongly (actually $I$ amplifies $\varphi$).

#### *2.1.1. Limitations to characterize nanoobjects*

**Geometrical limitation.** As an *a priori* condition, a mean free path of the emitting electrons must not exceed the size of the nanoobjects. In this case, the energy $E$, supplied to the electron to escape it, is limited with $L$, as shown in Fig. 2. Because of the above mentioned typical values of $\varphi$, the corresponding magnitudes of $L$ are placed in a range from 10 to 100 nm.

In this case the number of electrons (~$10^{-16}$… $10^{-15}$ Q/cm$^2$ [7]) that emit is from just $10^{-15}$%…$10^{-13}$ % of the emitter electron concentration (~$10^{23}$ cm$^{-3}$). This corresponds to the number of the excited electrons (photoelectron emission quantum yield <$10^{-7}$ [8]) < $10^{-8}$%…$10^{-6}$ % that, hopefully do not influence the properties of the measured nanoobject significantly. This means that the emission measurements do not give an important feedback to the tested object.

**Quantum mechanical limitation.** When the electron leaves the atom, the latter acquires location uncertainty $\Delta x$ because of the Heisenberg principle:

$$\Delta x \geq \frac{h}{4\pi\,\Delta p}, \tag{4}$$

where $h$ is the Planck constant, $h = 4.14 \times 10^{-15}$ eV sec and $\Delta p$ is the uncertainty of the atom's momentum $p$. To ensure that the emitted electron escapes from the nanoobject, the size of the latter should be larger than $\Delta x$.

Assuming that the atom had zero momentum before interaction with the photon, the "bumping" of the atom by the photon increases $p$ until the photon momentum value $h\nu/c$ ($c$ is the speed of the light). Therefore

$$\Delta p = \frac{h\nu}{c}.$$

Because the magnitude of the photon energy should be in accordance with the condition $h\nu \geq \varphi$, and typically $\varphi \cong 5$ eV, then one could estimate that $\Delta x \approx 0.2$ nm. However, in some cases, $\varphi$ could be rather small and therefore, correspondingly, $\Delta x$ increases.

*2.1.2. Instrumentation*

As it is noted above, the photon energy should be as close as possible to the electron work function $h\nu \approx\geq \varphi$. To supply the single photon electron emission mode and to avoid multiphoton effects as well as heating of the tested object, the flux of the photons should be rather weak. This stipulates small values of $I$. Because of this, very sensitive electron detectors must be used. Typically the secondary electron multipliers that have a noise of 0.1–1 electron/s are applied.

On the other hand, the value of $I$ should excess its uncertainty (to reach reliable measurements) that is minimally equal to $I^{1/2}$ as the current obeys the Poisson statistics. For the reasonable <10% uncertainty, if the current measurement unit is electron/s, we have

$$I^{1/2}/I < 0.1 \text{ or } I > 10^2 \text{ electron/s.}$$

The value of $\chi$ could be affected by ions/dipoles sorption/desorption on/from an emitter surface. This asks for stable and "passive" environment (preferably vacuum; $10^{-2}\ldots10^{-7}$ Pa [9,10]) for electron emission measurements.

Typically the surface of the emitter is not uniform in the sense of $\varphi$. As a result, a contact potential difference is induced between the surface areas. This decreases/increases $I$ from the places with lower/higher $\varphi$, correspondingly [8]. In fact, when characterization of $\varphi$ distribution is the aim of measurements, their results could become false. To avoid this, an external compensating electrical field ~$10^2\ldots10^3$ V/cm, directed from the surface to the detector, should be provided [8].

To select the photon energy, the eligible monochromator should be provided, too.

## 2.2. Dual electron emission

In the tested object that has an energy gap ($E_g$), electrons and holes are generated under the photons having the energy $h\nu_{ad} \geq E_g$. The excited charge carriers are mobile and therefore provide an opportunity to compensate the surface charge that is caused by the Fermi level pinning at the surface [11] and by adsorbed ions/dipoles [12]. The charge influences $\chi$. When photoelectron emission (PE) is provided and $h\nu_{ad}$ is switched on/off, keeping the condition $h\nu_{ad} < h\nu$, an increment ($\Delta I$) of $I$ is induced because of the $\chi$ shift. Such the technique is a dual emission (DE) mode of PE.

The values of $\Delta I$ may be calibrated in terms of the surface charge density, alteration of $\Delta I$ in time reflecting surface electrical potential relaxation, induced by switched on/off $h\nu_{ad}$ photon flux [13].

*2.2.1. Instrumentation*

The DE technique is similar to the one that is in use to detect PE; additional light source and monochromator to select suitable $h\nu_{ad}$ should be incorporated.

To minimize the influence of $h\nu$ on DE, the flux ($F$) of $h\nu$ should be in accordance with

$$F << F_{ad},$$

where $F_{ad}$ is the flux of $h\nu_{ad}$ photons.

## 2.3. Exoelectron emission

When heat is provided to the analysed object, relaxation processes within the surface layer, radiated with photons and emitting electrons, are induced; the values $N_i$, $N_f$, $\chi$, and $E_g$ alter and $I$ is expressed as

$$I(T) = K(T)[h\nu - \varphi(T)]^{m(T)},$$

where $T$ is temperature of the tested object; $T \neq \text{const}$.

This is the exoelectron photothermostimulated emission mode (PTSE) [10,14]. To reach PTSE, two steps are needed. First, a tested object at $T = T_i$ has to be provided with imperfections (because of technological processing, etc.). Their concentration should not be in a thermodynamically equilibrium state, if $T > T_i$. In this way increase of $T$ induces relaxation of imperfections, PTSE being supplied.

In some cases the relaxation processes could transfer the energy directly to the electron to escape it [10]; the photon is not necessary. Such mode is named thermostimulated exoelectron emission (TSEE).

The exoemission current $I_{EE}$ depends on $T$ as Fig. 3 demonstrates.

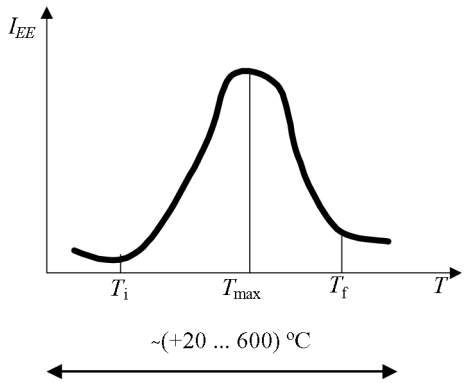


**Fig. 3.** Typical $I_{EE}$ spectrum; $T_i$ and $T_f$ are the initial and final temperatures of the spectrum, and $T_{max}$ is the temperature of its maximum.

TSEE is typically delivered because of the following mechanisms:

a) thermoionisation of local states, trapping electrons and belonging to the imperfections [10]; such a mechanism is available in materials with a wide $E_g$ and small $\chi$;
b) Auger transitions of electrons [10], from local electron traps of imperfections; this channel is available when $E_g > \chi$;
c) field emission from the electron traps by imperfections, because of the heat induced electrical polarization/depolarization of the emitting surface layer [15].

PTSE is provided as a single photon prethreshold PE, when heat causes:

a) modulation of the density of the electron emitting local states induced by imperfections [14,16];
b) shift of the Fermi level because of a) [16].

The above mechanisms fit materials, having the energy gap. Exoemission from metals is supplied perhaps from their surface oxides having properties of insulators or semiconductors [10].

For the ionization mechanism, $T_{max}$ corresponds to the ionization potential of the electron trap [16]. There are experimental evidences [10] that

$$I_{EE}(T) \sim \mathrm{d}C/\mathrm{d}T, \tag{5}$$

where $C$ is the concentration of relaxing imperfections.

The total emitted charge $(Q)$ is directly proportional to $C$ at $T_i$ [10,14]. The activation energy $(E_r)$ of relaxation for the simplest first order annealing reaction may be estimated as [10,14]

$$E_r = -kT \ln[I_{EE}(T)/N(T)], \tag{6}$$

where $k$ is the Boltzmann constant, $N(T) = \int_T^{T_f} I_{EE}(T)\mathrm{d}T$.

In the case of semiconductors, the exoemission spectrum is modified by annealing of the point type complexes of the defects, supplying single imperfections. Thus the reaction is represented by the build-up branch of the spectrum $(T_i < T < T_{max})$ [14].

For the first order reaction activation energy of complexes, annealing $(E_{act})$ is available from the formula (6) [14]. However, $T_f$ should be replaced with $T_{max}$ [14].

The build-down branch of the EE spectrum $(T_{max} < T < T_f)$ corresponds to the migration of the generated single imperfection to the surface of the specimen, because of the complexes dissociation due to annealing. An activation energy of migration $(E_m)$ in the case of uniformly distributed single defects within a specimen may be estimated from the formula [14]

$$E_m = -kT \ln \frac{I_{EE}(T_{max})}{I_{EE}(T)} \frac{\mathrm{d}\left[\frac{I_{EE}(T_{max})}{I_{EE}(T)}\right]}{\mathrm{d}T}. \tag{7}$$

*2.3.1. Instrumentation*

The above instrumentation to detect PE and DE fits also exoemission measurement conditions. However, heating of the tested object should be provided in addition. The temperature of the specimen should not lead to the situation, when a significant thermoelectron emission current is excited that is the noise for exoemission.

## 3. APPLICATIONS OF THE PRETHRESHOLD ELECTRON EMISSION SPECTROSCOPY

### 3.1. Characterization of semiconductors

Semiconductors are widely used in medicine to fabricate mico- and nanocircuits as pulse oximeters, weight scales, glucose meters, digital thermometers, pulse/ blood pressure monitors, electrocardiogram devices, insulin pumps, digital stethoscopes, scanning equipment (ultrasound, MRI, digital X-ray, PET, optical, others), bone replacing implants and grafts, etc.

Functional properties of the semiconductor depend on $E_g$, concentration of imperfections and their stability, relaxation rate of the electrical charges, etc.

The mechanical tensions at the nanolayers could strongly control $E_g$. Influence of any mechanical load on a negative increment of the silicon $E_g$ [17] was used to identify the location of the mechanical tension, induced in a Si surface nanolayer (100 nm) because of its local doping with boron [18]. A distribution of $I$, related to the tensions over the surface, is demonstrated in Fig. 4. A crown at the boundary of the image corresponds to concentrators of local tensions.

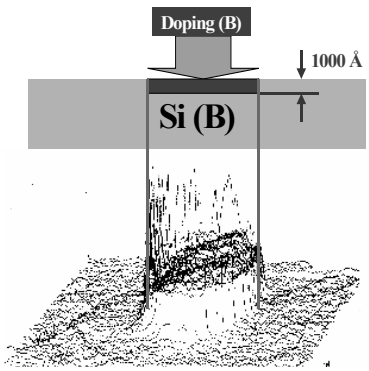


**Fig. 4.** Distribution of *I*, related to mechanical tensions over the Si surface [18].

The application of DE to identify $E_g$ value of the CdTe crystal surface layer (~1000 nm) was reviewed in [19]. Figure 5 provides $\Delta I$ as a function of $h\nu_{ad}$. The condition $h\nu_{ad} = E_g = 1.4$ eV was satisfied at $\Delta I = 0$.

A possibility to estimate the point type imperfections concentration, generated in a crystalline Si by $As^+$ ion radiation (50 keV), was demonstrated in [20]. Measured $Q$ value of PTSE (Fig. 4) was proportional to the delivered fluence ($F$) of ions (Fig. 6). The value of $Q$ was sensitive to $10^{-6}$ atomic % of As atoms concentration.

Tetra vacancies ($V_4$), generated in a monocrystalline Si nanolayer (~100 nm) because of $P^+$ ions (100 keV) radiation, were identified in [20]. The activation energy $E_r$ of complexes annealing was acquired from PTSE measurements due to calculations in Eq. (4). The value of $E_r$ decreased at high values of the delivered fluence (>$5.10^{14}$ $cm^{-2}$) because of interactions among $V_4$ (Fig. 7).

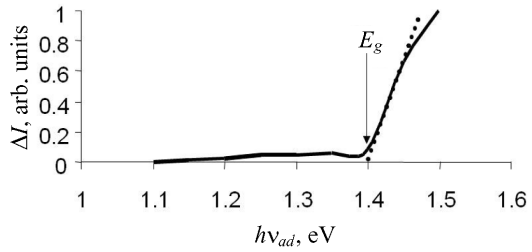


**Fig. 5.** The dependence of $\Delta I$ on $h\nu_{ad}$ for CdTe surface layer to identify its $E_g$ [19].

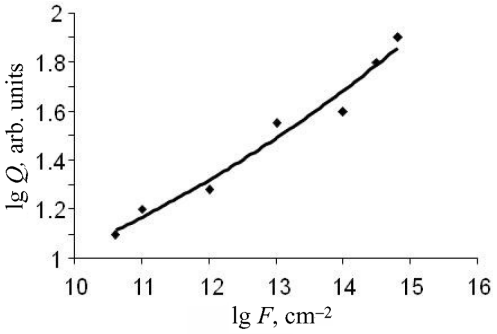


**Fig. 6.** Dependence of $Q$ on the $As^+$ ions fluence supplied to Si [21].

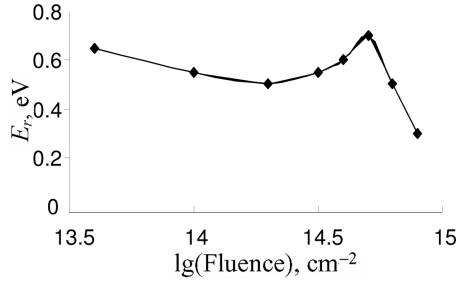


**Fig. 7.** $E_r$ of Si tetra vacancies as a function of $P^+$ ions fluence [20].

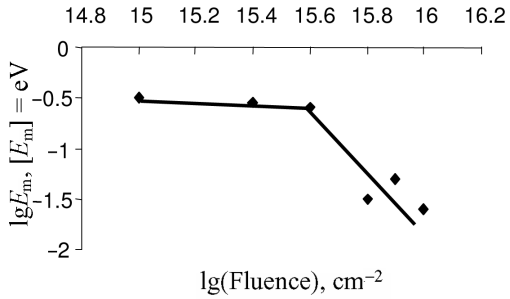


**Fig. 8.** $E_m$ of Si single defects as a function of electron fluence [20].

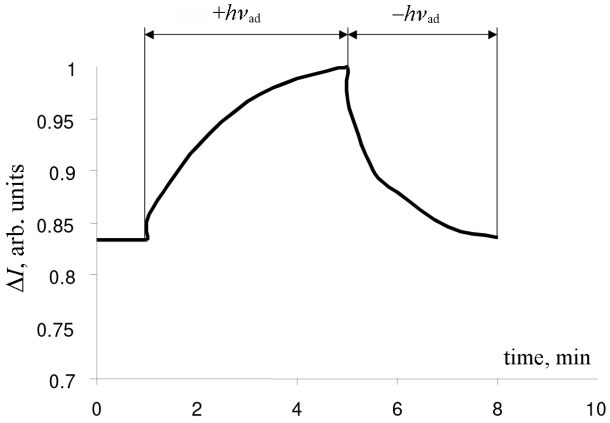


**Fig. 9.** $\Delta I$ of CdTe, influenced by $h\nu_d$, versus time [19].

The activation energy (7) of migration of single vacancies, generated in a monocrystalline Si owing to dissociation of the vacancy contending defect complexes, was identified in [20]. The complexes were induced due to electron radiation (5 MeV). The value of $E_m$ decreased at $F > 4 \times 10^{15}$ $cm^{-2}$ (Fig. 8) that was stipulated by interference of imperfections.

The DE mode, reviewed in [19] was applied to measure excitation and relaxation times of the charge at the CdTe crystal surface layer (~1000 nm). When the flux $F_{ad}$ was switched ($+h\nu_{ad}$) the value of $\Delta I$ increased in time (Fig. 9). However, when $F_{ad}$ was switched off ($-h\nu_{ad}$), $\Delta I$ relaxed. The estimated excitation and relaxation times were 3 and 2.5 min, respectively. One could assume that the detected times corresponded to the slow surface local states.

### 3.2. Nanofilms and interfaces

A possibility to apply PE to estimate the thickness of the $Si_3N_4$ nanofilm that is widely in use for nanoelectronics, (particularly medical electronics) was reviewed in [19]. The film was deposited with a variable thickness (5–100 nm) on the Si substrate. Because of simultaneous PE from both the film and the substrate, that are charac-

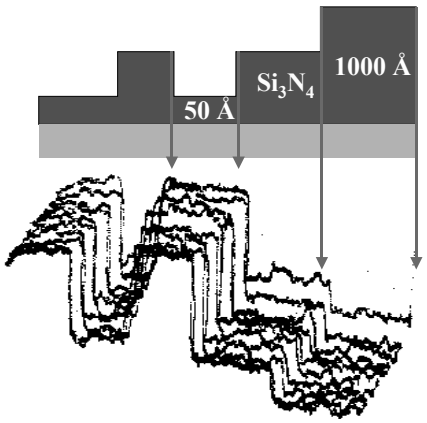


**Fig. 10.** PE current distribution as a function of the $Si_3N_4$ thickness[1] [19].

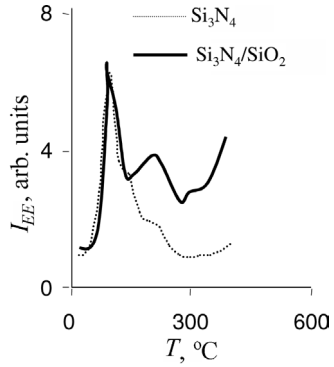


**Fig. 11.** $I_{EE}$ of the multilayer system $Si_3N_4/SiO_2$ [21].

terized with different $\varphi$, the value of $I$ depended on the thickness of the film. Figure 10 provides the $I$ distribution over the film surface.

Local states were identified at the interface between $SiO_2$ substrate and $Si_3N_4$ nanofilm (10 nm) [22]. The structure was radiated with weak electrons from the film side. The electrons were delivered with different energy to fill in the traps in the $Si_3N_4$ and $Si_3N_4/SiO_2$ interface. TSEE was detected after radiation. The $I_{EE}$ spectrum of $Si_3N_4$ significantly differs from the one, when the $Si_3N_4/SiO_2$ interface was radiated (Fig. 11).

### 3.3. Nanoparticles

Hydroxyapatite (HAP) nanoparticles are widely used for grafting of human bones, to assemble bioceramics, etc. The HAP surface should have specific properties to communicate with human cells. The electrical interaction is the important channel for this [22].

[1] With the courtesy of the author's colleague Dr. A. Balodis, Riga Technical University, Latvia.

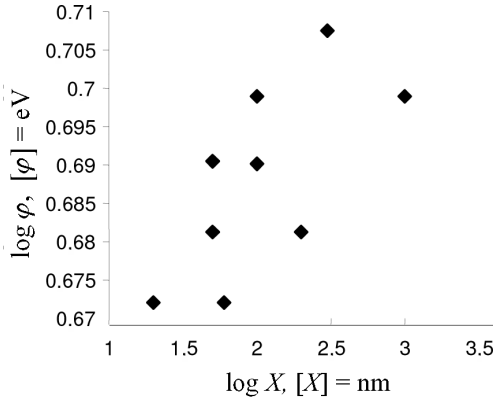


**Fig. 12.** Correlation of $\varphi$ and the size $X$ of nanoparticles [23,24].

It is known that mechanical surface tensions depend on the size of the sphere-like particles. This could influence the surface charge density, particularly in the case of ion crystals. As a result, the surface charge influences $\varphi$. Figure 12 [22] demonstrates the correlation between $\varphi$ and the size ($X$) of the hydroxyapatite nanoparticles. Computational simulation evidenced that this was stipulated by alteration of the electron state density, induced by protons of HAP [23].

The results were used to improve bone osteoblastic cell immobilization and proliferation for bioimplant HAP based ceramics [24].

### 3.4. Bone

The PE and DE were applied alongside with fluorescence measurements to explore electron states of the bovine bone [25]. The result presented in Fig. 13 evidence that the bone has semiconductor-like energy gaps.

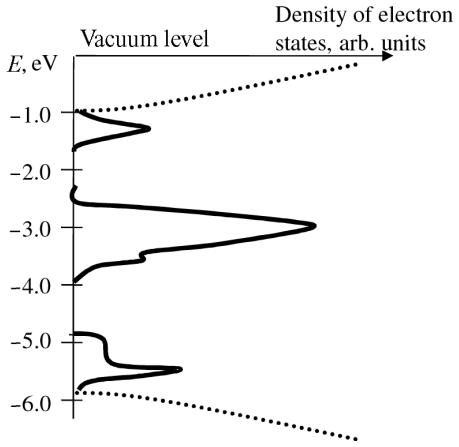


**Fig. 13.** Electron density of the states in bone [25].

This was used for the preclinical trial (animal experiments) to control healing of the bone defect. The bone surface was recharged, by the electrical charge carriers that were produced by photon radiation [26].

### 3.5. Gas and radiation sensing

Gas sensing and ionizing radiation are correspondingly employed for cancer diagnostics and therapy.

According to medical research, patients with cancer, diabetes and chronic obstructive pulmonary disease have very specific volatile organic compounds (VOC) in their exhaled gases [27–29]. Pathologically increased concentrations of VOC, such as benzene, acetone, toluene, pentane, and hexane, which are the metabolites of cancer cells, are very specific for oncology patients.

Crystalline Si specimens, prepared from Si (*p*-type conductivity, partial resistance 10 Ω cm, thickness 0.2 mm) and having a mirror-like polished surface, were deposited with benzene gases [30,31]. Absorption of gas molecules altered $\varphi$ that provided the $I$ response of PE. Gas absorption induced increment of the emitted charge indicated the volume of the molecules, attached to the wafer surface. Figure 14 demonstrates gases exposure dependence on the PE total emitted charge increment.

The sensitivity of the above approach was evaluated as $10^{-5}$ gram of benzene for 1 $cm^2$ of the adhering wafer surface [30,31].

Modern radiation therapy (RT) technologies and the needs of molecular and micro radiobiology have necessitated the detection of radiation, absorbed by micro/nano volumes. There are several reasons why nanodosimetry (ND) is of great importance: (i) biological effects caused by radiation depend on the dose, absorbed by nanosized DNA units; (ii) there is a trend in radiation therapy to apply high dose gradients (Gy/(μm…nm)), survival of the cells depends on the gradient value; (iii) nanoparticles as radiation scattering centres are expected to reach local micro-nano-scaled treatment that minimally influences risk organs/cells; (iv) radiation sensitive nanoparticles have the ability to penetrate from the environment to human body.

However, there are still no detectors that measure radiation in nanovolumes. Extrapolation of measurement results from the macro/micro to nano volumes, if the macro/micro sized currently available dosimeters are in use, provides a high uncertainty. This is connected with the Poisson statistics of the dose (D), its uncertainty $1/D^{1/2}$ strongly increasing, when the radiation absorbed volume is very small.

To fix the problem, a nanosized detector should be reached; nanoobjects are great candidates to become the dosimeter sensitive element. There are just a few of examples to get the nanodosimetry like sensor. For instance, a $TeO_2$-based thin film detector, having a thickness of 300 nm, has been demonstrated [32]. The electrical measurements of the radiation-induced properties of the detector material were employed to provide a readout of D [32,33]. However, annealing is required to renew a dosimeter [33]. In this case, electrical contact degradation [33] makes it difficult to use a thin film dosimeter repeatedly [33]. A contactless detector could be a good option for solving this problem.

The possibility to apply PE and PTSE for the nanodosimetry purposes is considered in [34]. An example is given, when PbS nanodots, imbedded in a $ZrO_2$ nanofilm, were employed [31,34]. The $ZrO_2$ : PbS films were fabricated using the sol-gel technique [35] with 20% concentration of PbS nanodots. The films were deposited on a glass substrate. Thickness of the films was 0.1–1 μm. Typical size of PbS nanodots was 2–4 nm. $ZrO_2$ : PbS films were radiated with 9 MeV electrons supplied from the medical linear accelerator. PE current was detected before and after radiation. The corresponding increment $\Delta[\mathrm{d}I/\mathrm{d}(h\nu)]$ recognized at $5.75 \pm 0.03$ eV correlated with the delivered dose (Fig. 15).

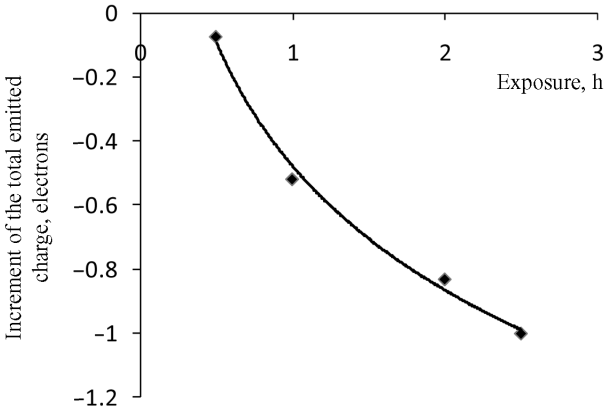


**Fig. 14.** Emitted charge increment versus exposure in benzene gas [32].

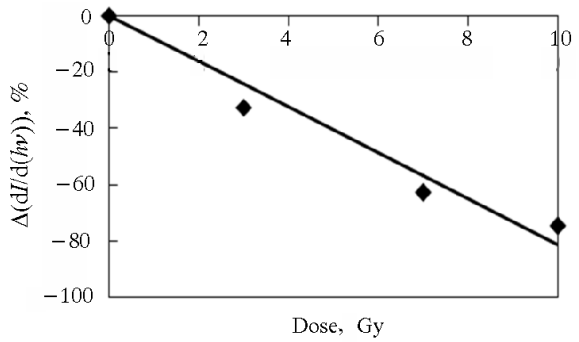


**Fig. 15.** Increment of $\Delta[\mathrm{d}I/\mathrm{d}(h\nu)]$ inspired by the delivered dose to the $ZrO_2$ : PbS nanofilms [31,34].

## 4. CONCLUSIONS

Prethreshold photo-, dual-, and exoemission are capable to supply a sensitive, contactless technique to characterize nanomaterials (concentration of point type imperfections, their annealing and migration, interaction; density of the electron states; thickness of nanofilms and interface/boundary between them; surface charge of the nanoparticles), gas and radiation sensing towards medical applications.

Weak emission ($\sim 10^{-16}\ldots10^{-15}$ Q/cm$^2$) of electrons does not give a significant feedback to measurements in the sense of the possible influence of the emission inducted electrical charge at the material surface.

To analyse nanoobjects, their size is limited with a range of 10–100 nm. The quantum mechanics limitation gives the uncertainty around 0.2 nm.

The minimal threshold concentration of the implanted atoms, particularly As in Si is around $10^{-6}$ atomic %.

The sensitivity of the chemical sensor, particularity to the benzene molecules could be achieved as $10^{-5}$ g per 1 cm$^2$ of the substrate surface.

## REFERENCES


1. http://www-scopus-com.resursi.rtu.lv/results/results.url?sort=plf-f&src=s&sid=9569DAF0CCF1B2A145F5D2FF6BABDDBA.WlW7NKKC52nnQNxjqAQrlA%3a40&sot=a&sdt=a&sl=23&s=Medical+gas+nanosensors&origin=searchadvanced&txGid=9569DAF0CCF1B2A145F5D2FF6BABDDBA.WlW7NKKC52nnQNxjqAQrlA%3a4; accessed 22 February 2014.
2. http://www-scopus-com.resursi.rtu.lv/results/results.url?sort=plf-f&src=s&sid=9569DAF0CCF1B2A145F5D2FF6BABDDBA.WlW7NKKC52nnQNxjqAQrlA%3a420&sot=a&sdt=a&sl=31&s=medical+radiation+nanodosimetry&origin=searchadvanced&txGid=9569DAF0CCF1B2A145F5D2FF6BABDDBA.WlW7NKKC52nnQNxjqAQrlA%3a42; accessed 22 February 2014.
3. http://www-scopus-com.resursi.rtu.lv/results/results.url?sort=plf-f&src=s&sid=9569DAF0CCF1B2A145F5D2FF6BABDDBA.WlW7NKKC52nnQNxjqAQrlA%3a540&sot=a&sdt=a&sl=42&s=medical+nanomaterials+and+characterization&origin=searchadvanced&txGid=9569DAF0CCF1B2A145F5D2FF6BABDDBA.WlW7NKKC52nnQNxjqAQrlA%3a54; accessed 22 February 2014.
4. Fomenko, V. S. *Emission Properties of Materials*. Naukova Dumka, Kiev, 1981 (in Russian).
5. Ibach, H. (ed.). *Electron Spectroscopy for Surface Analysis*. Springer-Verlag, New York, 1977.
6. Kinding, N. B. and Spicer, W. E. Band structure of cadmium sulphide photoemission studies. *Phys. Rev.*, 1963, **138**, A561–A576.
7. Dekhtyar, Yu. Emission of weak electrons towards sensing nanoobjects. In *Technological Innovations in Sensing and Detection of Chemical, Biological, Radiological, Nuclear Threats and Ecological Terrorism*. (Vokoshta, A., Braman, E., and Susman, P., eds). Springer, 2012, 171–178.
8. Dobrecov, L. N. and Gomoyunova, M. V. *Emission Electronics*. Nauka, Moscow, 1966 (in Russian).
9. Dekhtyar, Yu. D. and Sagalovich, G. L. Exoelectron emission of monocrystalline silicon and its practical application. *Proc. USSR Academy of Sci., Physical Ser.*, 1988, **52**, 1611–1613 (in Russian).
10. Kortov, V. S., Shifrin, V. P., and Gaprindashvili, A. I. Exoelectron spectroscopy of semiconductors and insulators. *Microelectronics*, 1975, **8**, 28–49 (in Russian).
11. Nesterenko, B. A. and Cnitko, O. V. *Physical Properties of Atomic Clean Surface of Semiconductors*. Naukova Dumka, Kiev, 1983 (in Russian).
12. Volkenstein, F. F. *Electron Processes on Semiconductors Surface During Chemosorption*. Nauka, Moscow, 1987 (in Russian).
13. Arvin, H., Bogucharska, T., Dekhtyar, Yu., Hill, R. M., Katashev, A., Pavlenko, A. et al. Electronic transitions and structural changes in bone. *Latvian J. Phys. Techn. Sci.*, 2000, **6**(S), 50–55.
14. Dekhtyar, Yu. D. and Vinjarskaja, J. A. Exoelectron analysis of amorphous silicon. *J. Appl. Phys.*, 1994, **75**, 4201–4207.
15. Rosenman, G. I., Rez, I. S., Chepelev, Yu. L., and Angert, N. B. Exoemission of defected surface of lithium tantalite. *J. Techn. Phys.*, 1981, **51**, 404–408 (in Russian).
16. Dekhtyar, Yu. D. *Exoelectron Spectroscopy of Point Type Defects in Semiconductors*. Riga Technical University, Riga, 1993 (in Russian).
17. Polyakova, A. L. *Deformation of Semiconductors and Semiconductor Devises*. Energiya, Moscow, 1979 (in Russian).
18. Balodis, A., Dekhtyar, Yu., and Sagalovich, G. Emission local testing of mechanical stresses in surface layer of silicon. *Proc. SPIE*, 1994, **2334**, 244–249.
19. Dekhtyar, Yu. Photo- dual and exoelectron spectroscopy to characterize nanostructures. In *Functionalized Nanoscale Materials, Devices, and Systems for Chem.-Bio Sensors, Photonics, and Energy Generation and Storage*. Springer, 2008, 169–183.
20. Dekhtyar, Yu. D., Noskov, V. A., Savvaitova, J. A., and Sagalovich, G. L. Generation and annealing of vacancy complexes in the monocrystalline Si surface layer. *Phys. and Techn. of Semiconductors*, 1990, **3**, 492–496 (in Russian).
21. Rosenman, G., Naich, M., Molotskii, M., Dekhtyar, Yu., and Noskov, V. Exoelectron emission spectroscopy of silicon nitride thin films. *Appl. Phys. Lett.*, 2002, **80**, 2743–2745.
22. Dekhtyar, Yu., Bystrov, V., Bystrova, A., Dindune, A. Yu., Katashev, A., Khlusov, I. et al. Engineering of hydroxyapatite cell adhesion capacity. *IFMBE Proc.*, 2012, **38**, 182–185.
23. Bystrov, V., Bystrova, N., Dekhtyar, Yu., Filippov, S., Karlov, A., Katashev, A. et al. Size depended electrical properties of hydroxyapatite nanoparticles. *IFMBE Proc.*, 2006, **14**, CD version. Springer, Seoul, 3149–3150.

24. Dekhtyar, Yu., Dvornichenko, M. V., Karlov, A. V., Khlusov, I. A., Polyaka, N., Sammons, R., and Zaytsev, K. V. Electrically functionalized hydroxyapatite and calcium phosphate surfaces to enhance immobilization and proliferation of osteoblasts *in vitro* and modulate osteogenesis *in vivo*. *IFMBE Proc.*, 2009, **25**, 245–248.
25. Arvin, H., Bogucharska, T., Dekhtyar, Yu., Hill, R. M., Katashev, A., Pavlenko, A. et al. Electronic transitions and structural changes in bone. *Latvian J. Phys. and Techn. Sci.*, 2000, **6**(S), 50–55.
26. Dekhtyar, Yu., Katashev, A., Katasheva, J., and Ozolante, I. Effect of optical radiation influence on bone defect reconstruction in rabbits. *IFMBE Proc.*, 2008, **20**, 357–360.
27. Wang, C. and Sahay, P. Breath analysis using laser spectroscopic techniques: breath biomarkers, spectral fingerprints, and detection limits. *Sensors*, 2009, **9**, 8230–8262.
28. Shirau, M. and Touhaza, K. The scent of disease volatile organic compounds of the human body related to disease and disorder. *J. Biochem.*, 2011, **3**, 257–266.
29. Mandis, A. The diagnostic potential of breath analysis. *Clin. Chem.*, 1983, **29**, 5–15.
30. Vaseashta, A., Braman, E., Susmann, P., Dekhtyar, Yu., and Perovicha, K. Sensors for water safety and security. *Surface Eng. Appl. Electrochem.*, 2012, **48**, 478–486.
31. Dekhtyar, Yu., Krumpane, D., Perovicha, K., Reisfeld, R., Romanova, M., Saraidarov, T., and Surkova, I. Electron emission standed nanodosimetry and gas detection. In *Advanced Sensors for Safety and Security* (Vaseashta, A. and Khudaverdyan, S., eds), pp. 173–180. Springer, Netherlands, 2013.
32. Maity, T. K., Sharma, S. L., and Chourasiya, G. The real-time gamma radiation dosimetry with $TeO_2$ thin films. *Radiat. Meas.*, 2012, **47**, 145–148.
33. Arshak, K. Thin and thick films of metal oxides and metal phthalocyanines as gamma radiation dosimeters. *IEEE Trans. Nucl. Sci.*, 2004, **51**, 2250–2255.
34. Dekhtyar, Yu. Emission of weak electrons: Dosimetry of nanovolumes. *Radiat. Meas.*, 2013, **55**, 34–37.
35. Sashchiuk, A., Lifshitz, E., Reisfeld, R., Saraidarov, T., Zelner, M., and Willenz, A. Optical and conductivity properties of PbS nanocrystals in amorphous zirconia sol-gel films. *J. Sol-Gel Sci. Techn.*, 2002, **24**, 31–38.

## Elektronide emissioonist põhjustatud nõrga voolu kasutamine nanomaterjalide iseloomustamisel ja gaaside ning kiirguse avastamisel, hinnates meetodi võimalikke meditsiinilisi rakendusi

Yuri Dekhtyar

Nanomaterjalide kiire areng avab laialdased võimalused nende kasutamiseks erinevates valdkondades ja meditsiin on üks neist. Nanomaterjale ja nanoseadmeid kasutatakse nii inimese kehas kui ka meditsiiniliste nanosensoritena. Materjalide usaldusväärseks kasutamiseks peab teadma nende omadusi. Nanomaterjalide ja nanosensorite iseloomustamiseks tuleb kasutada ka vastavat nanodimensioonis mõõteskaalat. Et mitte nanoobjekte mõõtmisel mõjutada, tuleks eelistada kontaktivaba tehnikat. Madala energiaga elektroni vaba teekond tahkes keskkonnas ligikaudu vastabki sellele vajalikule nanodimensioonis mõõteskaalale. Seega peaks madala energiaga elektronide baasil loodud kontaktivaba spektroskoopia olema hea meetod nii nanostruktuursete materjalide kui ka nanoandurite uurimisel. Nõrk elektronide emissioon materjalist ($\sim 10^{-16} \ldots 10^{-15}$ Q/cm$^2$) ei mõjuta oluliselt laengut selle materjali pinnal, kuna elektronide tihedus seal on suurusjärgus $10^{14}$ cm$^{-2}$. Käesolevas artiklis on antud ülevaade foto-, duaal- ja eksoemissioonidest ning nende kasutamise võimalikkusest nanoobjektide, nagu punktikujuliste pinnadefektide kontsentratsioon, nende parandamine ja migratsioon ning ka nanoosakeste pinnalaeng, iseloomustamisel. Samuti on käsitletud gaaside ja ioniseeriva kiirguse avastamist ning meetodi võimalikke meditsiinilisi rakendusi.